THE FORMATION AND EXTENT OF THE SOLAR SYSTEM COMET CLOUD

MARTIN DUNCAN
Scarborough College and Department of Astronomy, University of Toronto, West Hill, Ontario M1C 1A4, Canada

THOMAS QUINN AND SCOTT TREMAINE
Canadian Institute for Theoretical Astrophysics, University of Toronto, 60 St. George Street, Toronto, Ontario M5S 1A1, Canada
Received 11 May 1987; revised 16 July 1987

ABSTRACT

We present the results of numerical simulations of the origin and evolution of the solar system comet cloud. We assume that comets formed in the outer planetary region and that their orbits evolved to their current state through planetary perturbations, stellar encounters, and the Galactic tide. The evolution is followed using a hybrid integration scheme which directly integrates the regularized equations of motion for cometary orbits with large semimajor axes, while solving an energy-diffusion equation for more tightly bound orbits. Stellar encounters are introduced via a Monte Carlo approach using the impulse approximation. The simulations show that the formation of the comet cloud is driven by the interaction between planetary perturbations, which drive diffusion in semimajor axis a at constant pericentric distance q, and tidal torques, which change q at fixed a and thereby remove cometary perihelia from the planetary region. An inner edge to the cloud is found at ≈ 3000 AU—roughly the radius at which the timescales for the two effects are equal for comets formed in the Uranus–Neptune region. The density profile between 3000 and 50 000 AU is roughly a power law proportional to $r^{-3.5}$. The inner or Hills Cloud ($a < 20\,000$ AU) thus contains roughly five times as many comets as the classical Oort Cloud ($a > 20\,000$ AU), but comets from the inner cloud enter the inner planetary region only during brief comet showers triggered by the passage about every 100 Myr of a star which comes within 10^4 AU of the Sun (cf. Hills 1981). Our simulations suggest that the flux of comets during a shower may be as much as 20 times higher than the steady-state rate, but is unlikely to be larger, no matter how strong the perturbation.

I. INTRODUCTION

The modern era in the study of comet dynamics began with the celebrated paper by Oort (1950), in which he proposed that the Sun was surrounded by a reservoir or cloud of comets with semimajor axes a and energies $x \equiv 1/a$ in the range $0 < x \lesssim 10^{-4}$ AU^{-1} (our use of the term "energy" for x is a slight abuse of notation since the true orbital energy differs from x by the factor $-\frac{1}{2} G\mathcal{M}_{\odot} m$). Oort argued that stellar perturbations occasionally brought the perihelion distance q of a comet in the cloud into the region $q \lesssim 10$ AU, where planetary perturbations are important. In this region, the typical change in energy per perihelion passage due to planetary perturbations is greater than the initial energy of a comet in the cloud; hence the comet rapidly either (i) escapes from the solar system (as soon as $x < 0$) or (ii) diffuses to a much more tightly bound orbit. Oort suggested that the observed concentration of comets with energies in the range $0 < x \lesssim 10^{-4}$ AU^{-1} arose from comets entering the planetary system for the first time ("new" comets) with perihelion sufficiently small ($q \lesssim 2$ AU) that they are visible from the Earth, while the comets with energy $x \gtrsim 10^{-4}$ AU were once new comets but had already suffered perturbations on one or more previous perihelion passages.

Oort's model of the comet cloud has been modified and extended in several ways over the past decade: (i) Encounters with passing molecular clouds may have a perturbing influence on the comets which is comparable to that of stars (Biermann and Lüst 1978; Biermann 1978). However, the influence of molecular clouds is difficult to estimate because their parameters are so uncertain (Hut and Tremaine 1985), and the consistency of observations with models of the comet cloud that neglect molecular clouds suggests that they do not have a major qualitative influence on the evolution of the comet cloud. Moreover, most of our attention is focused on comets in orbits with $a \lesssim 10^4$ AU, which are relatively immune to molecular cloud perturbations because of adiabatic invariance. For these reasons, in a preliminary investigation such as this one it seems appropriate to neglect molecular clouds, and we shall do so throughout this paper. (ii) The Galactic tidal field exerts a torque on the cloud comets which can cause them to drift into the planetary region. It appears that the tidal torque dominates stellar perturbations as a source of new comets, contributing roughly 80% of the flux of new comets (Heisler and Tremaine 1986; Morris and Muller 1986; Heiser *et al.* 1987; Bailey 1986). (iii) Hills (1981) has observed that we should not generally expect to see any new comets unless the typical perihelion change due to stars and tides is large enough to bring the comet from outside the planetary system ($q \gtrsim 10$ AU) to inside the visibility zone ($q \lesssim 2$ AU) in one orbit. This condition can be shown to imply that new comets should have semimajor axes exceeding about 2×10^4 AU, which is satisfying close to the minimum semimajor axis actually observed in the concentration of comets near $x = 0$. Thus the minimum observed semimajor axis of new comets does not necessarily represent the inner edge of the comet cloud, and Hills stressed that the comet cloud may extend to much smaller radii and contain far more comets with $a \lesssim 2 \times 10^4$ AU than with $a > 2 \times 10^4$ AU. The comets in the inner cloud would only contribute to the flux of new comets during comet "showers" occurring after a particularly strong stellar perturbation. To distinguish the outer cloud, $a > 2 \times 10^4$ AU, which is directly observed through the new comets, from the hypothetical inner cloud, $a < 2 \times 10^4$ AU, we shall call the former the "Oort" Cloud and the latter the "Hills" Cloud. The relative population of the Hills and Oort clouds is perhaps the largest single uncertainty in our understand-

 0004-6256/87/051330-09$00.90

ing of the comet cloud; the population of the Hills Cloud may range from zero to more than 100 times that of the Oort Cloud.

Another major issue is the formation of the comet cloud. One appealing theory is that comets formed in the planetary system and were scattered out to the comet cloud by encounters with the planets (Oort 1950; Kuiper 1951). In this view, the outer parts of the solar accretion disk first condensed into small bodies composed of ices and rocks; some of these accreted to form Uranus and Neptune, while the remainder were repeatedly scattered by the growing planets until they reached semimajor axes large enough for tides and stellar perturbations to remove their perihelia from the planetary region, after which they are relatively immune to planetary perturbations. The bodies that reach "safety" in this way comprise the comet cloud that is present today.

Several competing theories of comet formation have been proposed (for example, that comets form in the outskirts of an extended solar nebula at distances of several hundred AU), but they will not be considered here (see Fernández 1985 for a review). Instead, we shall assume that comets are formed in the region of the outer planets and investigate the process by which cometary orbits evolve through planetary scattering and perturbations by stellar encounters and the Galactic tide. Our principal aim is to determine the relative efficiency of populating the Oort and Hills clouds and hence to determine, within the context of this formation scenario, the present relative cometary populations of these two regions. Before discussing the results of the detailed simulations, we present some rough timescale arguments in Sec. II which will delineate the key features of the evolution.

Our work is similar in many respects to a calculation carried out by Shoemaker and Wolfe (1984); the relation of our results to theirs is discussed in the conclusions.

II. TIMESCALES

The growth of the outer planets by accretion of small bodies has been investigated numerically by Fernández and Ip (1981, 1983, 1984). These simulations show that the growth time for Uranus and Neptune is very uncertain: depending on such factors as the presence of other large bodies and the existence of extended gaseous envelopes around the protoplanets, the growth time may range from $\approx 10^8$ yr to several times 10^9 yr or even longer. Even after the planets are formed, their long-term efficiency in scattering small bodies that do not make close approaches to the planets is difficult to determine. In view of these uncertainties, we shall not attempt to follow in detail the initial stages of the process by which the planets scatter small bodies from the protoplanetary disk into the comet cloud. Instead, we simply note that the evolution to large semimajor axis is almost always through repeated weak scatterings: hence every comet that will eventually enter the cloud must, at some time, have any given semimajor axis a_i, which we shall take to be $a_i = 100$ AU, and we may simply specify our initial conditions through the distribution of times, perihelia, and inclinations at which the comets first have semimajor axis a_i. We consider two limiting cases for the temporal distribution of the appearance of comets at a_i: (i) a "prompt" model, in which all of the comets are scattered out to a_i shortly after the formation of the solar system at $t = 0$; (ii) a "steady-state" model, in which the rate at which comets are scattered through a_i is constant in time. For simplicity, in both models we assume that all of the planets have their present masses at

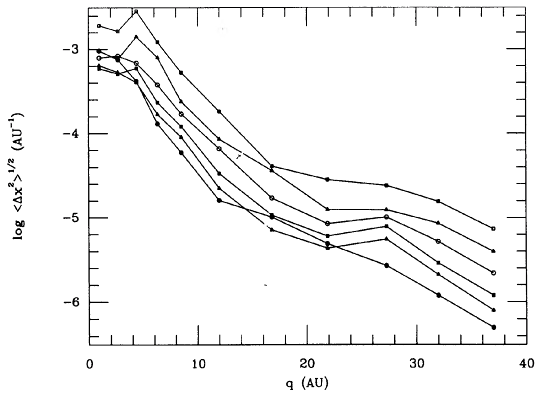

FIG. 1. The rms energy change per encounter for planetary perturbations is plotted as a function of perihelion distance. The light squares, light triangles, light circles, dark squares, dark triangles, and dark circles correspond, respectively, to inclination ranges relative to the ecliptic of 0°–30°, 30°–60°, 60°–90°, 90°–120°, 120°–150°, and 150°–180°. Each point is based on 3000 scatterings with random argument of perihelion.

all times, although another interesting model would be one in which the outer planets grew slowly to their present masses.

Once the semimajor axis $a \gtrsim a_i = 100$ AU, the scattering process becomes much simpler, for several reasons. First, the orbital period of the comet is sufficiently large [$P = 1000$ yr $(a/100\ \mathrm{AU})^{3/2}$] that the positions of the planets at successive perihelion passages may be considered to be uncorrelated; thus the planetary perturbations cause a random walk of the cometary orbital elements. Second, since the orbit is near parabolic, the probability distribution of the perturbations is independent of the semimajor axis of the comet, and depends only on the perihelion distance q, the inclination i, and the argument of perihelion ω. Figure 1, which is modeled after Fig. 1 of Fernández (1981), shows the root-mean-square (rms) energy change per passage, as a function of q and i. Each data point was obtained from the distribution of energy changes for 3000 comets with random values of ω. We have suppressed the dependence on ω because the energy change is not a strong function of ω for small inclinations, which are the most important in our discussion. Figure 1 is more fully discussed in Sec. IV.

The third reason why the scattering process is simple is that perturbations in q and i are much less important than perturbations in energy x. To see this, let $D(x)$ and $D(q)$ be the typical* energy and perihelion perturbations per perihelion passage of a comet with given q and i. Since both q and x undergo a random walk, the characteristic number of passages required for the energy to change by an order equal to itself is $N_x \approx [x/D(x)]^2$, and the typical perihelion change in N_x passages is $\Delta q \approx D(q) N_x^{1/2} \approx x D(q)/D(x)$. Similar expressions hold for the changes in i. In a typical case, say $i = 10°$ and $q = 25$ AU, we find $D(x) = 2.4 \times 10^{-5}$ AU^{-1}, $D(q) = 5.6 \times 10^{-3}$ AU, and $D(i) = 2.8 \times 10^{-4}$, and hence the typical changes in the other orbital elements over the

*The meaning of "typical" is not very well defined, since there are occasional close encounters with a planet which lead to large energy changes. However, our simulations indicate that close encounters contribute less than 30% to the rms energy change over the relevant number of orbital passages to be used in the arguments below. This point is discussed more fully in Sec. IV.

energy diffusion timescale are $\Delta q \approx 2$ AU$\times(100$ AU$/a)$, $\Delta i \approx 7° \times (100$ AU$/a)$. These are sufficiently small that both q and i can be taken to be approximately constant once $a \gtrsim 100$ AU.

Thus, for $a \gtrsim 100$ AU, planetary perturbations cause a random walk in energy x at constant perihelion q and inclination i. The nature of this random walk has been investigated by many authors. Yabushita (1980) shows that if $n(x,t)dx$ is the number of comets at time t with energies in the range $[x, x+dx]$ for given q and i, then n satisfies the diffusion equation

$$\frac{\partial n}{\partial \tau} = \frac{1}{2} x_0^{1/2} \frac{\partial^2 (n x^{3/2})}{\partial x^2}, \qquad (1)$$

where x_0 is arbitrary, $\tau = t/t_{\rm D}(x_0)$, and the diffusion time is

$$t_{\rm D}(x) \equiv \frac{2\pi}{D^2(x)} \sqrt{\frac{x}{G\mathscr{M}_\odot}} = 1\times 10^6\ {\rm yr}\left(\frac{10^4\ {\rm AU}}{a}\right)^{1/2} \left[\frac{10^{-4}\ {\rm AU}^{-1}}{D(x)}\right]^2. \qquad (2)$$

In Eq. (2), the diffusion timescale $t_{\rm D}$ is defined by the random-walk relation $t_{\rm D}(x) \equiv P(x) x^2/D^2(x)$. Notice that $t_{\rm D}$ decreases with semimajor axis as $a^{-1/2}$ (Fig. 2). Thus, a typical comet that reaches large semimajor axis will have spent most of its time close to the planetary region.

The Green's function corresponding to the initial distribution $n(x, t=0) = \delta(x - x_0)$ is

$$n(x,t) = \frac{4}{x\tau} \exp\left[-\frac{8}{\tau}\left(1 + \sqrt{\frac{x}{x_0}}\right)\right] I_2\left[\frac{16}{\tau}\left(\frac{x}{x_0}\right)^{1/4}\right], \qquad (3)$$

where I_2 is a modified Bessel function. The simple solution provided by Eq. (3) fails when the semimajor axis becomes too large, for several reasons:

(i) When the typical energy change per orbit $D(x)$ is comparable to x, the diffusion approximation fails.

(ii) Torques from the Galactic tide lead to changes in the perihelion distance q and hence $D(x)$ can no longer be considered fixed. The orbit-averaged rate of change of angular momentum due to tides is (Heisler and Tremaine 1986)

$$\frac{dJ}{dt} = -5\pi G \rho_0 a^2 e^2 \sin^2 I \sin 2\omega_{\rm G}. \qquad (4)$$

Here $\rho_0 \simeq 0.185\ \mathscr{M}_\odot\ {\rm pc}^{-3}$ is the mean density in the Galactic disk, I is the inclination relative to the Galactic plane, and $\omega_{\rm G}$ is the argument of perihelion relative to the Galactic plane. For highly eccentric orbits, $J \simeq \sqrt{2G\mathscr{M}_\odot q}$, and thus the timescale on which the perihelion distance changes by $\Delta q \ll q$ is

$$t_q \equiv \frac{(G\mathscr{M}_\odot)^{1/2} \Delta q}{5\pi G \rho_0 q^{1/2} a^2 \sin^2 I_e} = 1.3\times 10^7\ {\rm yr}\left(\frac{\Delta q}{10\ {\rm AU}}\right)\left(\frac{25\ {\rm AU}}{q}\right)^{1/2}\left(\frac{10^4\ {\rm AU}}{a}\right)^2, \qquad (5)$$

where we have set $e = 1$, replaced $\sin 2\omega_{\rm G}$ by its median absolute value, $1/\sqrt{2}$, and replaced the inclination I by its value for orbits in the ecliptic, $I_e = 60.2°$. The quantity t_q is plotted in Fig. 2. Yabushita's Green's function (3) is invalid whenever $t_q \lesssim t_{\rm D}$, where t_q is defined using $\Delta q \simeq 10$ AU since Fig. 1 shows that $D(x)$ changes substantially for Δq of this order. We also define the tidal torque return time $t_{\rm r}$ to be the time required for q to cycle to its maximum value and back under the influence of tidal torques alone. We find from numerical integrations that for initially low-inclination orbits starting near $q \approx 25$ AU, $t_{\rm r} \approx 1.5\times 10^9\ {\rm yr}(a/10^4\ {\rm AU})^{-3/2}$, with a variation of a factor of about 2, depending on the value of $\omega_{\rm G}$. The quantity $t_{\rm r}$ is also plotted in Fig. 2. Most of the time in the cycle is spent with q near its maximum.

(iii) Perturbations from passing stars lead to a random walk in the perihelion distance. The nature of this random walk over a timescale Δt depends on the impact parameter of the closest encounter during the interval. If the interval is sufficiently short that the minimum impact parameter is larger than the semimajor axis, that is, if

$$\pi n a^2 \langle v_{\rm r} \rangle \Delta t \lesssim 1, \qquad (6)$$

then the rms change in angular momentum is (Heisler and Tremaine 1986)

$$\langle (\Delta J)^2 \rangle^{1/2} \simeq 18\ G\rho_{\rm s} a^2 \Delta t. \qquad (7)$$

Here n and $\rho_{\rm s}$ are the number and mass density in stars, $\langle v_{\rm r} \rangle = 4\sigma/\sqrt{\pi}$ is the mean relative speed, and σ is the one-dimensional dispersion of the stars (we assume that on average the Sun has had the same rms velocity relative to the local standard of rest as other stars). Setting the rms change in angular momentum equal to $\sqrt{G\mathscr{M}_\odot/2q}\,\Delta q$, we find that the characteristic time for a perihelion change Δq is

$$t_* \simeq 0.04 \frac{(G\mathscr{M}_\odot)^{1/2} \Delta q}{G\rho_{\rm s} q^{1/2} a^2} = 2.2\times 10^7\ {\rm yr}\left(\frac{\Delta q}{10\ {\rm AU}}\right)\left(\frac{25\ {\rm AU}}{q}\right)^{1/2}\left(\frac{10^4\ {\rm AU}}{a}\right)^2 \qquad (8)$$

for $\rho_{\rm s} = 0.05\ \mathscr{M}_\odot\ {\rm pc}^{-3}$. Note that t_* has exactly the same functional form as t_q but a slightly larger coefficient; for this reason we have not plotted t_* separately in Fig. 2.

Equation (8) is only valid if the inequality (6) is satisfied for $\Delta t = t_*$, which requires

$$0.4\left(\frac{n\mathscr{M}_\odot}{\rho_{\rm s}}\right)\left(\frac{\sigma}{20\ {\rm km\ s}^{-1}}\right)\left(\frac{\Delta q}{10\ {\rm AU}}\right)\left(\frac{25\ {\rm AU}}{q}\right)^{1/2} \lesssim 1, \qquad (9)$$

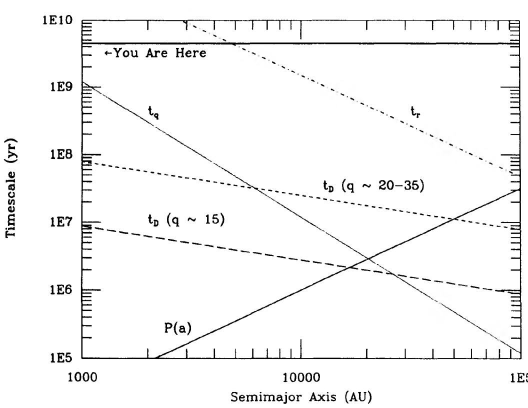

FIG. 2. The relevant timescales for the evolution of a solar system comet are plotted as a function of semimajor axis. $P(a)$ is the orbital period; $t_{\rm D}$ is the diffusion timescale for planetary perturbations (Eq. (2)); t_q is the tidal torquing time from the Galactic disk defined by Eq. (5) for $\Delta q = 10$ AU and $q = 25$ AU; $t_{\rm r}$ is the time required for Galactic tides to move a comet from minimum perihelion to maximum perihelion and back. The age of the solar system is indicated by the heavy horizontal line.

which is marginally valid in most cases of interest.

Thus, by a small margin, it appears that tides, rather than passing stars, are the dominant influence on cometary perihelia. This suggestion appears to be borne out by the numerical results presented below.

Now let us use these results to examine the evolution of a comet from an initial semimajor axis $a_i = 100$ AU, perihelion $q = 25$ AU, and low inclination. According to Fig. 1, $D(x) \simeq 2\times10^{-5}$ AU^{-1}, and hence the energy-diffusion time is $t_D \simeq 2.5\times10^8$ yr. As the comet random walks to larger semimajor axis, the energy-diffusion time decreases as $a^{-1/2}$, while the perihelion changes on a timescale that decreases as a^{-2}. From Eqs. (2) and (5), we conclude that $t_q < t_D$ for $a \gtrsim 6000$ AU (see Fig. 2).

Thus we expect the comet to random walk in energy at fixed perihelion until its semimajor axis reaches about 5000 AU. At this point, the tidal field will either decrease its perihelion to $q \lesssim 15$ AU, where the random walk in energy will proceed much more swiftly, or increase its perihelion to $q \gtrsim 35$ AU, in which case the perihelion has left the planetary zone and the comet has reached the comet cloud and safety from planetary perturbations. The comet will again approach the planetary region after a time $t_r \simeq 2\times10^9$ yr, but in that interval stellar perturbations will change the perihelion enough so that the comet is unlikely to re-enter the region of strong planetary perturbations.

These simple considerations suggest that the distribution of comets in the comet cloud is largely set by the competition between planetary perturbations and the Galactic tide, and that, in particular, the inner edge of the comet cloud is at the semimajor axis where the energy-diffusion time t_D and the timescale for perihelion change t_q become equal. However, the processes involved are sufficiently complex that the crude timescale arguments of this section must be supplemented by numerical models. Numerical modeling of the evolution of cometary orbits is greatly simplified by the following observation: comets with semimajor axes $a_i = 100$ AU must random walk at fixed q and i out to $a \approx 5000$ AU before they are substantially affected by tides or passing stars. Hence, the origin of the comet cloud can be determined by starting the numerical computations with an ensemble of comets at, say, $a_i = 2000$ AU rather than at $a_i = 100$ AU, since all potential cloud comets must pass through this state with nearly the same perihelion and inclination that they had at $a = 100$ AU. In the following section, we discuss numerical models of such an ensemble.

The validity of starting the integrations at $a_i = 2000$ AU rather than $a_i = 100$ AU has been checked by integrating a small number of comets ($N = 60$) with $a_i = 100$ AU and $q_i = 20$ AU. Each orbit was integrated until either (i) the comet reached semimajor axis $a > 2000$ AU, (ii) the comet was ejected, or (iii) the number of integrations steps exceeded 5×10^6, corresponding to about 10^5 orbits. We found that roughly 10% of the comets were ejected, 40% reached 2000 AU, and 50% stayed near $a = 100$ AU. Less than 5% of the comets had semimajor axes between 200 and 2000 AU when the integration was terminated. The perihelia of the comets reaching 2000 AU never exceeded 24 AU. These results confirm that comets evolve from $a = 100$ AU to $a = 2000$ AU with nearly fixed perihelion, and that very few comets are present between $a = 200$ AU and $a = 2000$ AU at any time. The interval 100 AU $< a <$ 2000 AU can be thought of as a nearly leakproof pipeline connecting the planetary region to the comet cloud region.

III. NUMERICAL METHOD

The study of the evolution of cometary orbits over the lifetime of the solar system presents a challenging numerical problem. Comets presently in the Oort Cloud have executed at least $\approx 10^3$ orbits during that time, often with large eccentricities, implying a force variation of several orders of magnitude over each period. The problem is exacerbated by the premise discussed above that the current cloud originated from a much more tightly bound population of comets on eccentric orbits which may have required 10^4 to 10^7 orbital periods to evolve to their current status.

The early stages of this evolution are adequately described by the diffusion equation (1). The purpose of the present paper is to investigate numerically the intermediate and late stages of this process, i.e., those regimes in which planetary perturbations, the Galactic tide, and encounters with passing stars are all potentially important. The numerical integration scheme must be able to handle extremely eccentric orbits ($e > 0.9999$) with very high accuracy. We have therefore adopted a scheme that is a generalization of that suggested by Stiefel and Schiefele (1971) for the restricted three-body problem with an additional conservative perturbing potential. In particular, the regularization of the equations of motion used in this method (see below) proves to be crucial to an accurate treatment of the orbits.

Since the dynamical influence of the terrestrial planets is easily shown to be negligible for all but extremely rare close encounters, we consider a model solar system comprised of the four giant planets revolving about the Sun in circular, coplanar orbits of zero inclination. The dominant contribution to the Galactic tidal field is that of the Galactic plane, which we model as a slab of density $\rho_0 = 0.185\ \mathcal{M}_\odot\ \mathrm{pc}^{-3}$ inclined at an angle of 60.2° to the ecliptic (Bahcall 1984; see also Heisler and Tremaine 1986).

The equations of motion in the barycentric frame are

$$\ddot{\mathbf{r}} = -\frac{G\mathcal{M}_\odot}{|\mathbf{r}-\mathbf{r}_\odot|^3}(\mathbf{r}-\mathbf{r}_\odot) - G\sum\frac{\mathcal{M}_p(\mathbf{r}-\mathbf{r}_p)}{|\mathbf{r}-\mathbf{r}_p|^3} - \nabla V. \tag{10}$$

In Eq. (10), $\mathbf{r}$, $\mathbf{r}_\odot$, and $\mathbf{r}_p$ are the barycentric positions of the comet, the Sun, and planet p, respectively, and $V = 2\pi G\rho_0 z_G^2$ is the Galactic tidal potential, where z_G is the component of $\mathbf{r}$ perpendicular to the Galactic plane.

Equation (10) can be rewritten using the barycentric definition $\mathcal{M}_\odot\mathbf{r}_\odot = -\Sigma\,\mathcal{M}_p\mathbf{r}_p$ in a form suitable for regularization:

$$\ddot{\mathbf{r}} = -\frac{G\mathcal{M}_T\mathbf{r}}{r^3} + \mathbf{P} - \nabla V, \tag{11}$$

where $r \equiv |\mathbf{r}|$, $\mathcal{M}_T \equiv \mathcal{M}_\odot + \Sigma\,\mathcal{M}_p$, and the "perturbing force" $\mathbf{P}$ is

$$\mathbf{P} \equiv -G\mathcal{M}_\odot\left(\frac{1}{\Delta_\odot^3} - \frac{1}{r^3}\right)(\mathbf{r}-\mathbf{r}_\odot) - G\sum\mathcal{M}_p\left(\frac{1}{\Delta_p^3} - \frac{1}{r^3}\right)(\mathbf{r}-\mathbf{r}_p), \tag{12}$$

where $\Delta_\odot \equiv |\mathbf{r}-\mathbf{r}_\odot|$ and $\Delta_p \equiv |\mathbf{r}-\mathbf{r}_p|$.

Introducing a new spatial 4-vector, $\mathbf{u}$, and a new independent variable s by means of the Kustaanheimo-Stiefel (K-S) matrix $L(\mathbf{u})$, such that $\mathbf{x} = L(\mathbf{u})\mathbf{u}$ and $ds = r\,dt$, Eq. (11) becomes (Stiefel and Schiefele 1971)

$$\mathbf{u}'' = -\frac{h}{2}\mathbf{u} + \frac{r}{2}L^{\mathrm{T}}(\mathbf{u})(\nabla V + \mathbf{P}), \tag{13}$$

where $' \equiv d/ds$, L^{T} is the transpose of the K-S matrix, and $h \equiv G\mathscr{M}_{\mathrm{T}}/r - \frac{1}{2}v^2 - V$. In the integration scheme, Eq. (13) is supplemented by the relations

$$t' = r = \mathbf{u}\cdot\mathbf{u} \text{ and } h' = -2\mathbf{u}'\cdot L^{\mathrm{T}}\mathbf{P}. \tag{14}$$

Equations (13) and (14) have the well-documented advantage over Eq. (10) that, in the absence of planetary perturbations, the equations of motion are those of a harmonic oscillator with a time-invariant frequency related to the energy but independent of the orbital eccentricity. We shall show that the numerical stability of the equations is maintained even in the presence of reasonably large perturbations.

The solar system contribution to the acceleration in Eq. (11) decomposes at large distances into a monopole term modified by a quadrupole term reflecting the finite extent of the system. At a distance $r_s \equiv 150$ AU the quadrupole term is $\approx 10^{-6}$ of the monopole contribution and adiabatic invariance guarantees that the net effect of neglecting the quadrupole term is negligible. As a result, once orbits pass beyond r_s, the solar system can be treated as a point mass at the barycenter, thereby avoiding the calculation of the planetary perturbation. The planetary perturbations, with the correct planetary phases, are reinstated whenever the comet re-enters the region $r < r_s$.

A fraction of the comets will random walk via planetary perturbations to tightly bound orbits with $a \lesssim 500$ AU and periods $\lesssim 10^4$ yr. The evolution of these orbits for several billion years by the methods described above would be prohibitively costly in CPU cycles, but these comets cannot be ignored since they may subsequently random walk back to large semimajor axes and enter the comet cloud. However, inside 500 AU the tidal torquing and stellar perturbations are negligible, so that the orbital evolution is well described by the energy-diffusion equation (1). This equation can be solved for an initial delta function in energy (subject to appropriate boundary conditions) to give the probability distribution in energy at any given time of a comet with a specified initial semimajor axis a_i.

Thus we proceed by initializing a set of cometary orbits in the same semimajor axis, say 2000 AU, and integrating the orbits directly using our regularization scheme. Any comet that reaches some more tightly bound orbit, say $a = 500$ AU, is removed from the integration and, at a time determined randomly from the probability distribution just described, is either reinserted at 2000 AU or is deemed to have become a tightly bound comet with $a < 100$ AU, at which time the approximation of energy diffusion at constant q breaks down and the integration from that comet is stopped. Once the comet is reinserted at 2000 AU, the integration is resumed as before until either 4.5×10^9 yr have elapsed or the comet is ejected.

Note that we have included in our simulations only the compressive component of the Galactic tidal field that is due to the Galactic disk. At heliocentric distances on the order of a parsec ($\approx 200\,000$ AU), the tidal field of the Galaxy in the equatorial direction establishes an outer limit to the solar system (Antonov and Latyshev 1972; Heisler and Tremaine 1986). Thus any comet that passes beyond 1 pc is deemed to have been tidally stripped and is removed from the simulation.

The stellar perturbations are incorporated by a Monte Carlo procedure described in more detail by Heisler *et al.* (1987). Our treatment uses the same assumptions regarding the mass spectrum, velocity dispersions, and number densities of the perturbers, and uses the impulse approximation to compute the relative velocity increment imparted to the comet as the result of an encounter. In practice, the stellar parameters relevant to the encounters are generated prior to a set of comet integrations and the orbital integrations are used to determine the comet's position and velocity at the relevant encounter time. No stellar perturbations are applied in the rare cases where the encounter timescale exceeds the comet orbital period, since adiabatic invariance implies that in these cases the perturbation will be much smaller than that predicted by the impulse approximation.

A fourth-order Runge-Kutta scheme was used to integrate the regularized equations. Using the timestep criteria described below, a full-scale simulation with all four planets, tides, and stars included requires about 0.3 s per orbit on a Sun 3/160 with Floating Point Accelerator board. The Sun is about three times faster than a VAX 11/780 with FPA, but, nonetheless, the simulations described below required about four months of CPU time on a dedicated Sun 3.

Extensive tests of the code have been performed with each of the perturbations acting alone. These tests show:

(i) In the absence of perturbations it was found that with roughly 60 steps per orbit, even when the eccentricity was as large as 0.99999, the energy of the orbit deviated by roughly one part in 10^{11} per orbit and the pericenter remained constant to one part in 10^6. Thus, millions of orbits can be reliably followed in the unperturbed case.

(ii) To maintain accuracy in the planetary region, at least 50 steps were taken when the comet was interior to r_s. In addition, the timestep was reduced still farther by a factor that depended on the ratio of the perturbing forces to the central force. This allowed for careful treatment of close encounters and resulted in a reduction of at least an order of magnitude in the step size when this ratio was of order unity. As a check on the scheme, several cases were run in which Jupiter was the only planet and a comet was integrated starting at $a = 100$ AU and $q = 4$ AU. After one hundred orbits the Jacobi integral (which is exactly conserved for the three-body system considered here) had changed by less than one part in 10^5.

(iii) The tidal-perturbation calculations were checked by running cases without planets and comparing the results with a numerical integration of the orbit-averaged equations of Heisler and Tremaine (1986). The agreement was good to one part in 10^3 with the discrepancy probably lying in the orbit averaging rather than the regularized scheme.

IV. RESULTS

Before turning to the full simulations, we briefly discuss the scattering experiments used to obtain Fig. 1. The results of these experiments were used in Sec. II to estimate timescales, and were used in the full simulations to obtain the diffusion timescale t_{D} [Eq. (2)] for comets reaching $a < 500$ AU, which are then followed by the diffusion equation until they reach $a = 2000$ AU. Since the timescale for this process is short ($\lesssim 3 \times 10^8$ yr) the simulation is quite insensitive to the exact value of t_{D} and the details of the diffusion process.

The calculation of the rms energy change $D(x)$ for parabolic encounters with a range of q and i used the same parameters as Fernández (1981) except that we have added two new sets of points at $q = 32$ and 37 AU in order to show the beginning of an abrupt decrease in $D(x)$ beyond 35 AU. Our results are in excellent agreement with those of Fernández when close encounters as defined by him* are excluded, but we do not find as marked an increase in $D(x)$ when close encounters are included. Our simulations show that, over a few thousand scatterings, close encounters increase the rms energy change by 20%–40%, while Fernández quotes increases of factors of 2–3 for low-inclination orbits. We feel that our results are likely to be more accurate since they rely on a precise orbital integration rather than the "sphere of influence" method used by Fernández. Our simulations confirm the result of Everhart (1968) that close encounters produce a tail proportional to Δx^{-3} in the distribution of energy changes. This tail produces a weak divergence in the rms energy change which is proportional to $\sqrt{\log (N)}$, where N is the number of scatterings. We have verified that this dependence is present by computing $D(x)$ for $N = 200$, 3000, and 30 000 scatterings. The calculated rms energy changes increased by about 40% over the range studied. The values shown in Fig. 1 are for $N = 3000$, which is roughly the appropriate number for the situation we are examining.

We now turn to the results of the complete simulations and examine the interplay among the perturbing influences that determine the properties of the comet cloud. In our most complete set of runs, we began with seven sets of about one thousand comets with initial semimajor axes of 2000 AU, inclinations of 18° and pericenters of 5, 10, 15, 20, 25, 30, and 35 AU. Each orbital integration was halted at 4.5×10^9 yr or earlier if the comet was either ejected, reached a radius $r > 1$ pc, or diffused into a tightly bound orbit ($a < 100$ AU). Many of the runs were repeated with one or more of the parameters altered in order to test the sensitivity of our results to the initial conditions. We shall see that the qualitative features of the evolution are remarkably robust.

Figure 3 shows the random walk in q and a for a typical comet that survives for the age of the solar system. It begins with $q = 20$ AU and $a = 2000$ AU. Note that the evolution is at roughly constant q for $a \lesssim 6000$ AU and at roughly constant a for $a \gtrsim 10\,000$ AU. There are several loops in q caused by the galactic tide. This particular comet is drawn back down to ≈ 3500 AU by planetary perturbations when its pericenter is tidally torqued back into the planetary region, a relatively rare occurrence.

Table I shows, for a given initial q, the percentage of comets that have attained each of the possible end states by 4.5×10^9 yr. The results are consistent with the timescale arguments of Fig. 2. In particular, comets with pericenters less than about 15 AU are unlikely to survive for the age of the solar system—the planetary perturbations are so large that the tides do not have time to torque them out of the planetary region before they are ejected. On the other hand, those with initial q between 15 and 35 AU are delivered to safety with reasonably high efficiency: roughly 30% of the comets survive.

The evolution of the spatial distribution of the survivors is illustrated in Fig. 4. It shows the distribution of our sample as seen from the Galactic plane after 10^7, 10^8, 10^9 and 4.5×10^9 yr have elapsed. Note that the ecliptic is inclined at

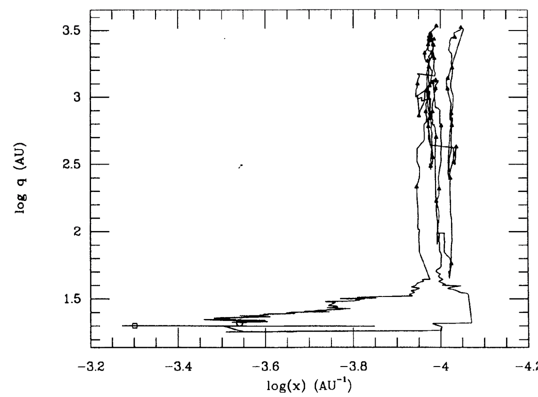

FIG. 3. The evolution in semimajor axis and perihelion is displayed for a typical comet. One data point is plotted per orbit. The comet started with a semimajor axis of 2000 AU and a perihelion of 20 AU (light square) and ended after 4.5×10^9 yr at the light circle. A triangle is plotted every 10^8 yr.

an angle of $\approx 60°$ to the Galactic plane and it is the Galactic tides and stellar perturbations that randomize the spatial distribution at large distances. The dotted circle in each snapshot is at a radius of 20 000 AU, indicating the inner edge of the classical Oort Cloud. It is evident from Fig. 4 that the distribution after 10^8 yr is still biased toward the ecliptic for orbits with $a \lesssim 10^4$ AU. However, by 10^9 years, the distribution is isotropic for $a \gtrsim 2000$ AU, and roughly 20% of the survivors are in the Oort Cloud, with the remainder populating the Hills Cloud. Between 10^9 and 4.5×10^9 yr, the total number of survivors decreased by a factor of ≈ 2, but the relative populations of the two clouds remained essentially unchanged.

For quantitative analyses of the overall distribution of surviving comets, we assume that the initial number density of perihelia was proportional to $q_i^{-1.0}$. (This is based on the assumption that the initial surface density in the solar nebula was proportional to r^{-2} and that the perihelion of a comet is approximately conserved in the initial phases of the scattering process. In fact, most of our results are insensitive to the initial perihelion distribution since the final semimajor-axis distributions (Fig. 7) have similar shapes at different q's.) Since our sample has equal numbers of comets at equal intervals in q, we simply weigh the contribution of each comet to the total by $q_i^{-1.0}$. Figure 5 shows the evolution of the mean inclination of the orbits with respect to the ecliptic as a function of semimajor axis. The dashed curve in Fig. 5 represents the weighted average of the cosines of the inclination of all surviving comets at $t = 10^9$ yr as a function of x. For $a \gtrsim 10^4$ AU, the mean is near zero, indicative of a random distribution. However, more tightly bound orbits retain a bias toward low-inclination orbits. The solid curve in Fig. 5 represents the same distribution at $t = 4.5 \times 10^9$ yr, and it is seen that the inclinations are random for $a \gtrsim 5000$ AU.

Figure 6 shows the mean value of the square of the orbital eccentricity as a function of x at $t = 10^9$ yr (dashed line) and $t = 4.5 \times 10^9$ yr (solid line). There is a bias toward radial (high-eccentricity) orbits at $t = 10^9$ yr for $a \lesssim 3000$ AU. At $t = 4.5 \times 10^9$ yr, the mean e^2 is everywhere very close to the value of 0.5 expected for an isotropic velocity distribution.

In Fig. 7(a) we plot the fraction of comets with energy greater than x as a function of x at $t = 10^9$ yr. Results are

*Fernández defines a close encounter to occur when a comet enters the "sphere of influence" of a planet. This is a spherical volume, centered on the planet, of radius $r_I = (\mathscr{M}_p/2\mathscr{M}_\odot)^{1/3} r_p$, where $\mathscr{M}_p$ and $\mathscr{M}_\odot$ are the masses of the planet and the Sun and r_p is the orbital radius of the planet.

TABLE I. Probable end states of comets.[a]

Initial perihelion (AU)	Planetary ejections	Stellar ejections	$r > 1$ pc	$a < 100$ AU	Survivors
5	0.84	0.02	0.04	0.09	0.02
10	0.73	0.01	0.15	0.06	0.06
15	0.45	0.05	0.21	0.05	0.24
20	0.46	0.02	0.17	0.06	0.29
25	0.44	0.01	0.16	0.05	0.34
30	0.41	0.01	0.15	0.04	0.40
35	0.35	0.03	0.13	0.04	0.41

[a] The bins with initial perihelia from 5 to 30 AU are calculated from a set of one thousand comets. The bin with initial perihelion of 35 AU is calculated from a set of 716 comets. In all cases the initial semimajor axis was 2000 AU and the initial inclination was 18°.

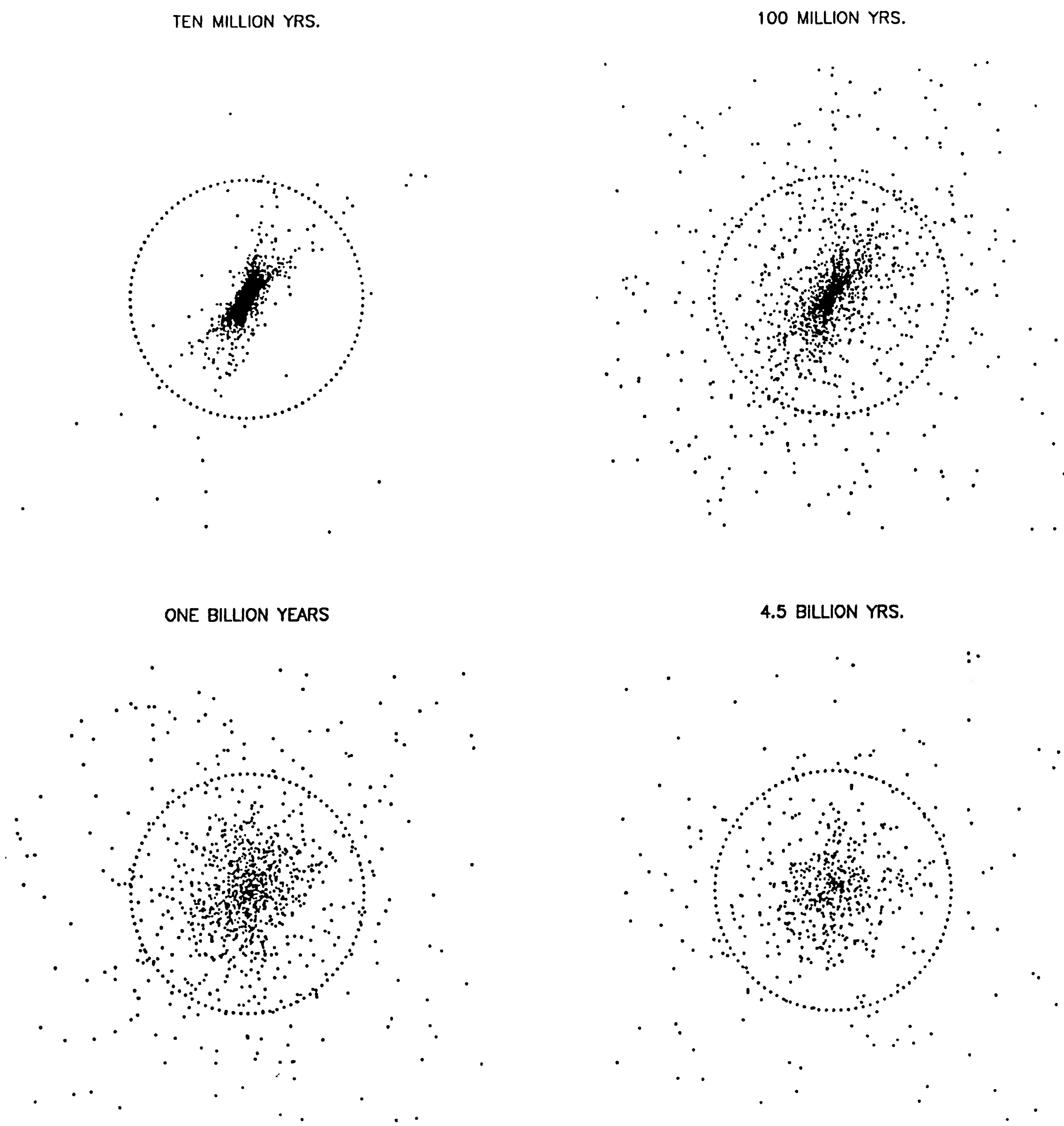

FIG. 4. The distribution of the comets in space is projected onto a plane for several different times. The plane $z = 0$ is parallel to the galactic plane. The dotted circle denotes a radius of 20 000 AU, indicating the inner edge of the classical Oort Cloud.

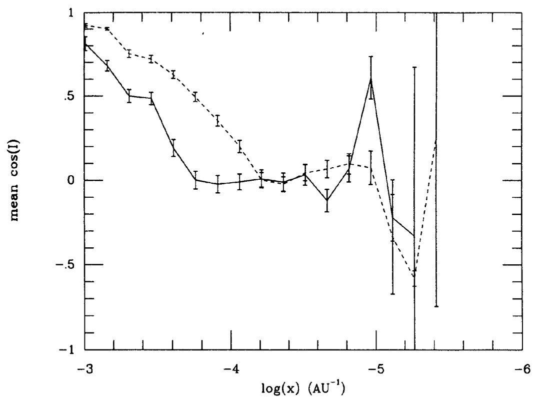

FIG. 5. The mean of the cosine of the inclination of comets to the ecliptic is plotted as a function of semimajor axis. The solid line corresponds to 4.5×10^9 yr and the dashed line to 1.0×10^9 yr.

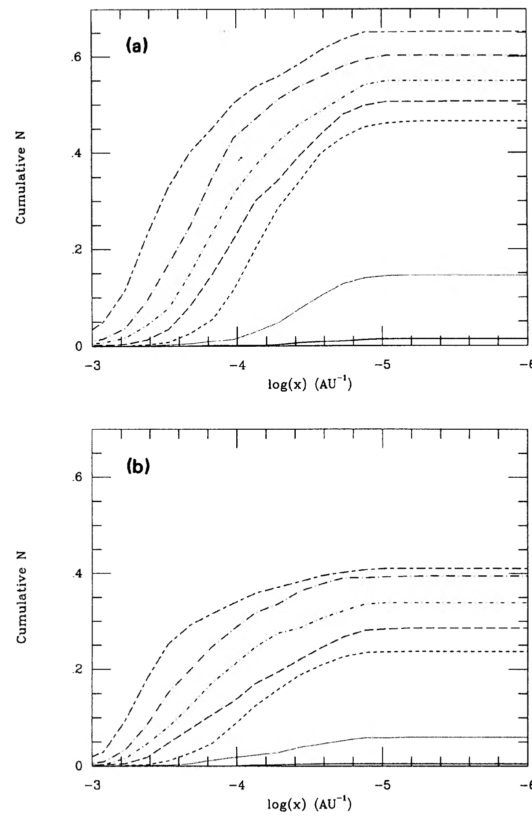

FIG. 7(a). The cumulative number of surviving comets as a fraction of the initial number of comets is plotted against semimajor axis at a time of 1×10^9 yr. The solid, dotted, short-dashed, long-dashed, dot-short-dashed, dot-long-dashed and long-short-dashed lines correspond to initial perihelia of 5, 10, 15, 20, 25, 30, and 35 AU, respectively. (b) The same quantities as in (a) are plotted at a time of 4.5×10^9 yr.

shown separately for each set of initial perihelia. Figure 7(b) shows the same quantities after 4.5×10^9 yr. These results confirm the qualitative predictions of the timescale arguments in Sec. II—the inner edge of the population of surviving comets is given roughly by the radius at which the timescale for tidal torquing equals the energy-diffusion timescale for the initial pericenter q_i. Since the energy-diffusion timescale increases with increasing q_i, we expect, and indeed find, that the inner radius of the surviving population decreases with increasing q_i.

Figure 8 shows the cumulative distribution of the surviving comets at $t = 10^9$ yr (dashed line) and $t = 4.5\times10^9$ yr (solid line). This distribution was obtained using the weighting scheme described above but the results are insensitive to the assumed initial distribution, since most of the survivors are comets with initial perihelia in the range 15 AU $\lesssim q_i \lesssim 35$ AU, for which the final energy distributions are very similar. We see from Fig. 8 that approximately 80% of the comets lie in the Hills Cloud, $a < 20\,000$ AU, and the Hills Cloud has a rather sharp inner cutoff at ≈ 3000 AU. The resulting spatial density of comets is proportional to r^{α} with $\alpha = -3.5 \pm 0.5$ for 3000 AU $\lesssim r \lesssim 50\,000$ AU.

All of the above results are for the "prompt" model for appearance of the comets at the initial semimajor axis. We have also investigated the "steady-state" model by examining the distribution of comets that have been integrated for a random time uniformly distributed between 0 and 4.5×10^9 yr. The characteristics of the distribution of semimajor axes in the steady-state model are similar to those of the prompt

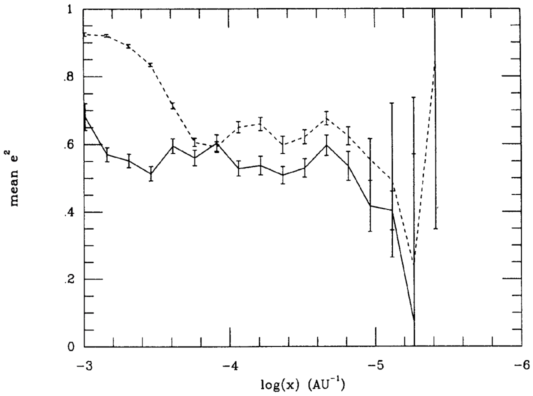

FIG. 6. The mean-square eccentricity is plotted as a function of semimajor axis. The solid line corresponds to 4.5×10^9 yr and the dashed line corresponds to 1.0×10^9 yr.

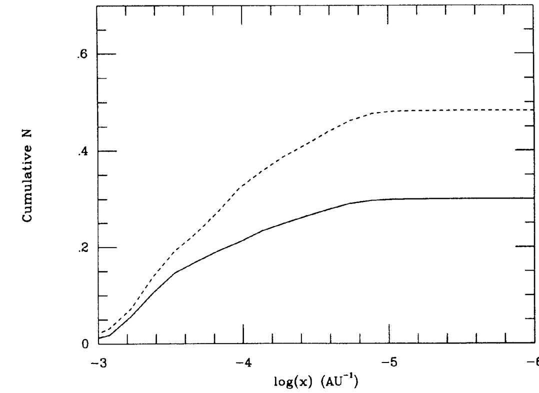

FIG. 8. Assuming an initial distribution in perihelion $\propto q^{-1.0}$, the cumulative distribution of comets is plotted against semimajor axis. The dashed line is for a time of 1.0×10^9 yr, and the solid line is for 4.5×10^9 yr.

model, with the curves falling between the curves for 1×10^9 and 4.5×10^9 yr in the prompt model.

The origin of the steady-state flux of new comets is, of course, the Oort Cloud, and comets from the Hills Cloud only enter the inner planetary region directly during a comet shower. The upper limit to the flux of comets during a shower can be obtained by assuming that a close stellar encounter fills the loss cylinder at every radius in the Hills Cloud. We find that in this case the flux will be ≈ 20 times higher than the steady-state flux for a shower duration of 3×10^6 yr. This flux is at least an order of magnitude lower than many previous estimates of the flux in a shower (e.g., Hills 1981). It is interesting to note in this context that Kyte and Wasson (1986) have measured the sea-floor iridium concentration for the period from 33 to 67 Myr ago. They find an increase by a factor of ≈ 13 near the Cretaceous–Tertiary boundary (66 Myr ago). Thus our model of the Hills Cloud predicts that the strongest possible comet showers would yield an iridium enhancement within a factor of 2 of the magnitude seen at the Cretaceous–Tertiary boundary.

V. CONCLUSIONS

We have simulated the formation of the solar system comet cloud and have studied its subsequent evolution over an interval equal to the age of the solar system. We have employed a numerical scheme that accurately computes the perturbations on cometary orbits from the giant planets, Galactic tides, and random passing stars. Assuming that the comets formed in the outer planetary region, we have shown that the formation of the current comet cloud was driven mainly by an interaction between planetary perturbations and torquing due to Galactic tides. This interaction produced an inner edge to the cloud at ≈ 3000 AU—the radius where the timescales for the two processes are comparable.

The comet orbital inclinations and eccentricities are found to be randomized by perturbations from the tides and passing stars for semimajor axes $a \gtrsim 5000$ AU. The density profile between 3000 and 50 000 AU is roughly proportional to $r^{-3.5}$, so that $\approx 20\%$ of the surviving comets lie in the classical Oort Cloud ($a > 20\,000$ AU). We estimate that the flux of comets into the inner solar system during a comet shower initiated by the close passage of a passing star may be as much as 20 times higher than the steady-state rate, but is unlikely to be much larger. This result is consistent with the iridium deposition rate determined from the geological record.

Our results are based on the assumption that all comets formed in the planetary region. Many authors (see Fernández 1985) have suggested that an extensive belt of comets may be present outside the planetary system. Such a belt does not evolve dynamically over the lifetime of the solar system and hence cannot be addressed by the methods used here.

After this work was nearly complete, we learned that similar calculations had been carried out by Shoemaker and Wolfe (1984). The principal differences are that (i) Shoemaker and Wolfe used Öpik's sphere-of-influence approximation to compute the planetary perturbations, rather than integrating the orbits numerically; (ii) they started the comets from near-circular orbits within the planetary region rather than from near-parabolic orbits with perihelia in the planetary region. Shoemaker and Wolfe's calculation suggests that the Hills Cloud is substantially more massive than that we have estimated: they find that 85% of the comets have semimajor axes $a < 10\,000$ AU and 70% have $a < 5000$ AU (our numbers are 70% and 50%). We believe that the discrepancy may arise from their use of the Öpik approximation, which substantially underestimates the planetary perturbations at perihelia outside Neptune's orbit (Fig. 1).

We would like to thank Julia Heisler for making available to us her Monte Carlo code for simulating stellar perturbations, Man Hoi Lee for programming assistance, and Gene Shoemaker for helpful discussions. This research was made possible by a Special Research Grant from the Connaught Fund at the University of Toronto and was assisted by funding from the Natural Sciences and Engineering Research Council.

REFERENCES

Antonov, V. A., and Latyshev, I. N. (1972). In *The Motion, Evolution of Orbits, and Origin of Comets,* IAU Symposium No. 45, edited by G. A. Chebotarev and E. I. Kazimirchak-Polonskaya (Reidel, Dordrecht), p. 341.
Bahcall, J. N. (1984). Astrophys. J. **276**, 169.
Bailey, M. E. (1986). Nature **324**, 350.
Biermann, L. (1978). In *Astronomical Papers Dedicated to Bengt Strömgren,* edited by A. Reiz and T. Anderson (Copenhagen Observatory, Copenhagen), p. 327.
Biermann, L., and Lüst, R. (1978). Sitz. ber. Bayer. Akad. Wiss. Mat.-Naturw. Kl.
Everhart, E. (1968). Astron. J. **73**, 1039.
Fernández, J. A. (1980). Mon. Not. R. Astron. Soc. **192**, 481.
Fernández, J. A. (1981). Astron. Astrophys. **96**, 26.
Fernández, J. A. (1985). In *Dynamics of Comets: Their Origin and Evolution,* edited by A. Carusi and G. B. Valsecchi (Reidel, Dordrecht), p. 45.
Fernández, J. A., and Ip, W.-H. (1981). Icarus **47**, 470.
Fernández, J. A., and Ip, W.-H. (1983). Icarus **54**, 377.
Fernández, J. A., and Ip, W.-H. (1984). Icarus **58**, 109.
Heisler, J., and Tremaine, S. (1986). Icarus **65**, 13.
Heisler, J., Tremaine, S., and Alcock, C. (1987). Icarus **70**, 269.
Hills, J. G. (1981). Astron. J. **86**, 1730.
Hut, P., and Tremaine, S. (1985). Astron. J. **90**, 1548.
Kuiper, G. P. (1951). In *Astrophysics,* edited by J. A. Hynek (McGraw-Hill, New York), p. 357.
Kyte, F. T., and Wasson, J. T. (1986). Science **232**, 1225.
Morris, D. E., and Muller, R. A. (1986). Icarus **65**, 1.
Oort, J. H. (1950). Bull. Astron. Inst. Neth. **11**, 91.
Shoemaker, E. M., and Wolfe, R. F. (1984). Lunar Planet. Sci. **XV**, 780.
Stiefel, E. L., and Schiefele, G. (1971). *Linear and Regular Celestial Mechanics* (Springer, New York).
Yabushita, S. (1980). Astron. Astrophys. **85**, 77.

THE ASTRONOMICAL JOURNAL

FOUNDED BY B. A. GOULD
1849

VOLUME 94 **November 1987 ~ No. 1582** NUMBER 5

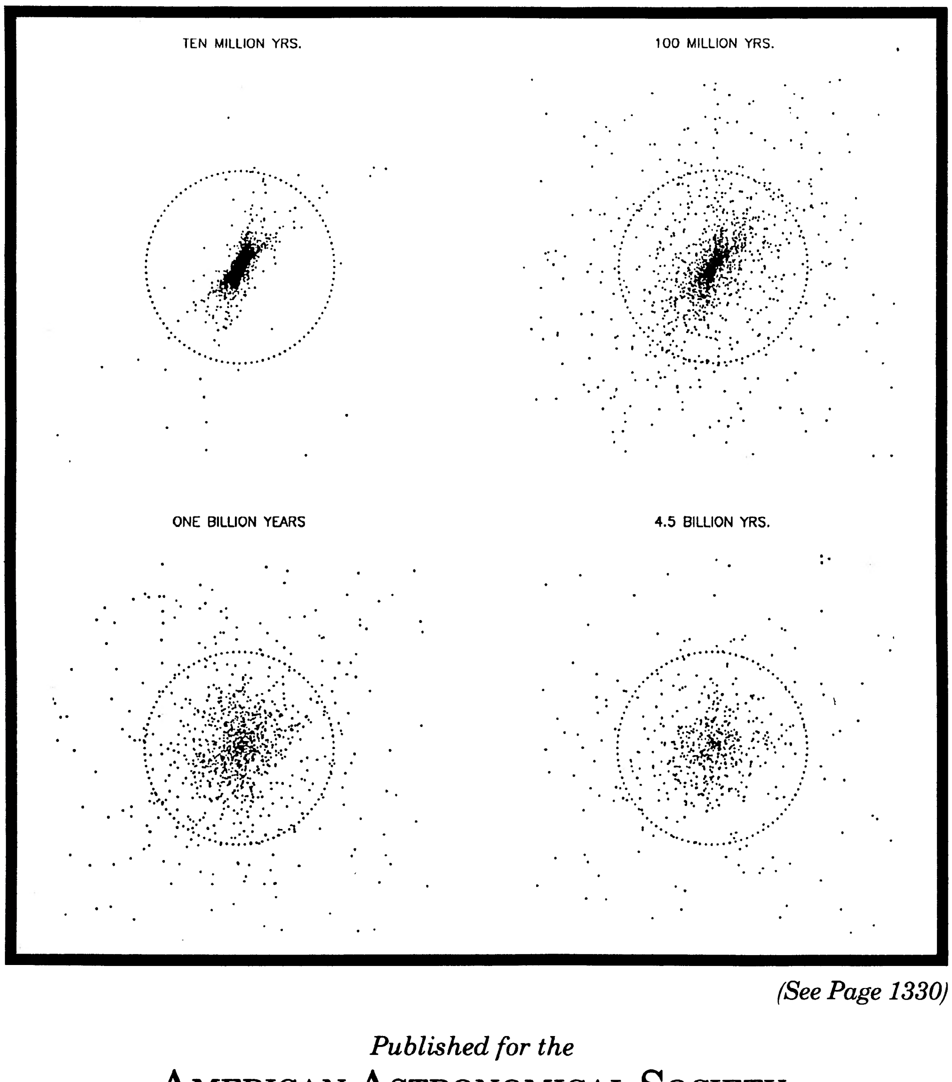

(See Page 1330)

Published for the
AMERICAN ASTRONOMICAL SOCIETY
by the
AMERICAN INSTITUTE OF PHYSICS